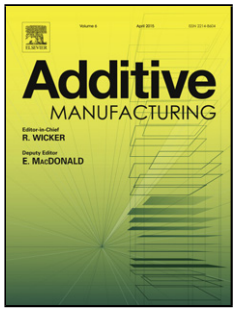

Benchmarking Spatial Resolution in Electronic Imaging for Potential In-Situ Electron Beam Melting Monitoring

Hay Wong, Derek Neary, Eric Jones, Peter Fox, Chris Sutcliffe

PII: S2214-8604(19)30050-8

DOI: https://doi.org/10.1016/j.addma.2019.100829

Article Number: 100829

Reference: ADDMA 100829

To appear in:

Received Date: 15 January 2019

Revised Date: 10 June 2019

Accepted Date: 5 August 2019

Please cite this article as: Wong H, Neary D, Jones E, Fox P, Sutcliffe C, Benchmarking Spatial Resolution in Electronic Imaging for Potential In-Situ Electron Beam Melting Monitoring, *Additive Manufacturing* (2019), doi: https://doi.org/10.1016/j.addma.2019.100829

Benchmarking Spatial Resolution in Electronic Imaging for Potential In-Situ Electron Beam Melting Monitoring

Authors: Hay Wong[a], Derek Neary[a], Eric Jones[b], Peter Fox[a], Chris Sutcliffe[a]

[a]School of Engineering, University of Liverpool, The Quadrangle, Brownlow Hill, United Kingdom L69 3GH

[b]Jones Consultancy, Ardlahan, Kildimo, Co. Limerick, Ireland

Corresponding author's email: Hay Wong – hay.wong@liv.ac.uk

Abstract

Electron Beam Melting (EBM) is an increasingly used Additive Manufacturing (AM) technique employed by many industrial sectors, including the medical device and aerospace industries. In-process EBM monitoring for quality assurance purposes has been a popular research area. Electronic imaging has recently been investigated as one of the in-process EBM data collection methods, alongside thermal / optical imaging techniques. So far, the disseminations focus on the design of an electronic imaging system and the ability to generate electronic images in-process, experiments are yet to be carried out to benchmark one of the most important features of any imaging systems – spatial resolution. This article addresses this knowledge gap by: (1) proposing an indicator for the estimation of spatial resolution which includes the Backscattered Electrons (BSE) information depth, (2) estimating the achievable spatial resolution when electronic imaging is carried out inside an Arcam A1 EBM machine, and (3) presenting an experimental method to conduct a knife edge test with the EBM machine. Analyses of experimental results indicated that the spatial resolution was of the order of 0.3 to 0.4mm when electronic imaging was carried out at room temperature. It is believed that by disseminating an analysis and experimental method to estimate and quantify spatial resolution, this study has contributed to the on-going quality assessment research in the field of in-process monitoring of the EBM process.

Keywords: Electron Beam Melting; In-Process Monitoring; Quality Control; Electronic Imaging; Spatial Resolution

1. Introduction

1.1 Introduction to Electron Beam Melting (EBM)

EBM is an Additive Manufacturing (AM) technique that makes use of an accelerated electron beam to melt metallic powder on a layer-by-layer basis, forming components based on the geometries of the imported three dimensional (3D) Computer Aided Design (CAD) models [1]. When the electron beam raster-scans across a preheated powder bed in a predefined pattern, melt tracks are solidified and fully-dense cross-sections of the desired component are formed. This process is repeated with the additional requirement that the solid is also partially re-melted to ensure adequate bonding between the underlying and newly formed layers ensuring that near full density in components is achieved. The EBM process offers reduced thermal residual stress in components [2] and high level of design freedom [3]. It is thought that the technique shows great promise in the manufacturing of orthopaedic implants and aerospace components [4]. However, due to process issues including non-uniform powder layer deposition [5], peeled-off metallisation on the processing area [6], and component defects including, porosity within melted area [5], balling along melt tracks [7] and delamination of processed layer [8], the widespread adoption of EBM in industry is hindered unless a rigorous EBM process monitoring and validation system is available for real-time control [9].

1.2 Technology Gaps in Electronic Imaging Spatial Resolution Analysis in EBM Monitoring

Two academic research groups have attempted to employ feedback electronic imaging as the data collection method for monitoring the EBM process. At the Friedrich-Alexander-University of Erlangen-Nürnberg (Germany), Arnold et al [10] introduced a Backscattered Electrons (BSE) imaging system. A BSE detector was mounted inside the electron beam column of a modified Arcam S12 EBM machine (Arcam AB / GE Additive, USA), above the EBM processing chamber. Electronic images were generated from the BSE signals originated from elastic collision between the incident machine electron beam and the processing area. Detection of in-layer porosity within a set of EBM manufactured components was carried out via electronic image analysis. Moreover, results were compared with optical microscopy and X-ray Computed Tomography (CT) images generated post-process, in order to validate the observations from the in-process electronic images. The second group working in the same field is from the University of Liverpool (UK). Wong et al [11] developed a custom

electronic imaging system prototype and interfaced it with an Arcam A1 EBM machine (Arcam AB / GE Additive, USA). The prototype consisted of a SE/ BSE sensor, signal amplifier, data-logger, and image generation software [11]. The group investigated the prototype capabilities, and presented findings including, magnification range, the selection of image Field-of-View (FOV) [12], and the influence of temperature on the quality of electronic images [13]. In spite of the research efforts made by these two groups, no information is available regarding (1) the achievable spatial resolution, and (2) how to quantify and benchmark this parameter for an electronic imaging system operating inside an EBM machine. This study aims to address these knowledge gaps by estimating and evaluating experimentally the achievable spatial resolution of an electronic imaging system prototype when interfaced with an EBM machine.

1.3 Spatial Resolution Evaluation for High Energy Beams

Spatial resolution is an important feature of an imaging system as it dictates how capable a system is to reveal topographical details of an imaged target [14]. Reimer [15] stated that electron beam size and resolution are inter-related in electron microscopy, and spatial resolution is limited by the machine electron beam size. Thus, this study postulates that the beam size can serve as an indicator for the estimation of the achievable spatial resolution. There are various ways to define the size of a high energy beam, i.e. laser, electron beam, which includes but not limited to, Full Width Half Maximum (FWHM) [16], $1/e^2$ width [17], D4σ width (second-moment width) [18], and knife edge width [19, 20]. In this pilot study, owing to the simplicity of the experimental setup, the knife edge resolution has been selected as the definition of the spatial resolution for the electronic imaging system interfaced with an EBM machine. In a knife edge test, when a high energy beam moves perpendicularly to and across sharp edges (indicated by the red dotted lines, as shown in Fig. 1(a)), the beam intensity spatial distribution profile, i.e. the Edge Spread Function (ESF), illustrated in Fig. 1(b), is observed [15]. The knife edge spatial resolution of the beam can be defined as the spatial width measured between two beam intensity values of 25% and 75% of the maximum intensity value [15].

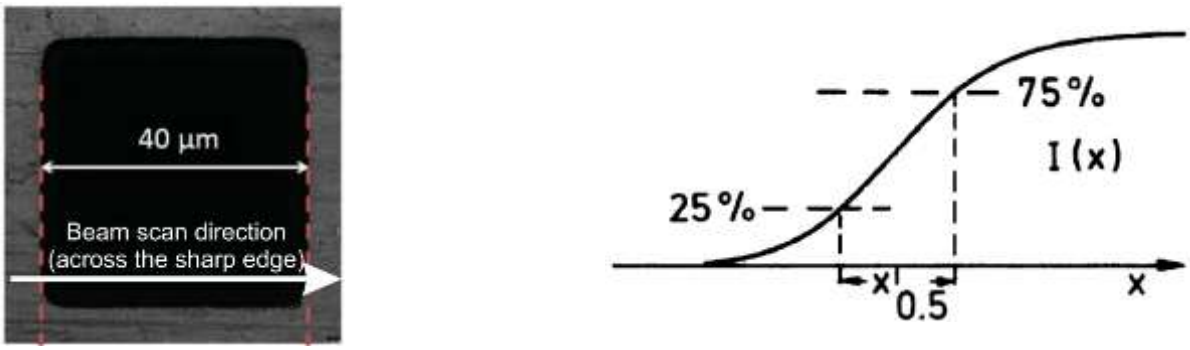

(a) TEM grid with 40µm hole (adapted to show scan direction)[21]

(b) Resolution is the spatial width of values 25% to 75% of maximum value [15]

Fig. 1 Sharp edge and the definition of spatial resolution from an ESF

2. Materials and Methods

This section first presents the estimation on spatial resolution, and then describes the experimental setup for the investigation of spatial resolution in details.

2.1 Theoretical Analysis of Spatial Resolution

This article postulates that for the evaluation of spatial resolution in electronic imaging, in addition to the electron beam diameter, the extra width incurred from the feedback electron information depth should also be taken into account. In electronic imaging, the feedback electron signal consists of Secondary Electrons (SE) and Backscattered Electrons (BSE), as shown in Fig. 2(a) [15]. These electrons are generated from the imaging target at different information depths, with BSE originating from deeper inside the imaging target, as indicated by the electron-specimen interaction volume in Fig. 2(b).

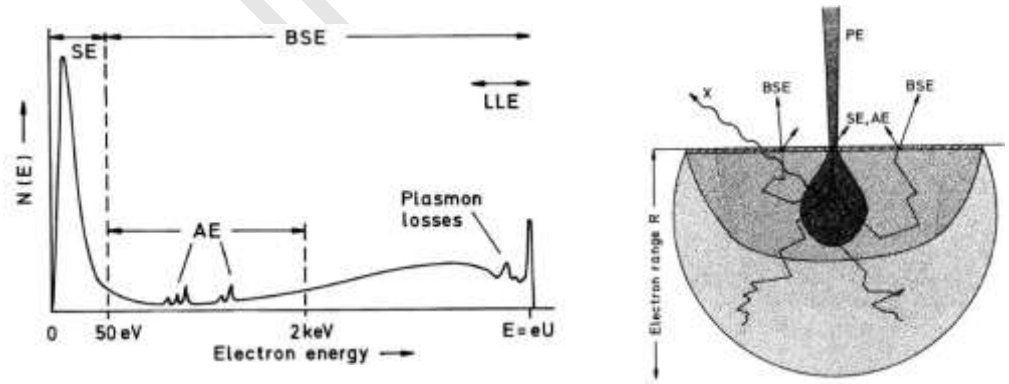

(a) Energy spectrum of feedback electrons

(b) Interaction volume, information depth

Fig. 2 Electron-material interaction and products [15]

In this study, the spatial resolution of an electronic imaging system is defined as the diameter of the Arcam A1 EBM machine electron beam with the maximum additional width incurred from the information depth, i.e. the BSE information depth. Fig. 3 illustrates this concept and the definitions of beam size and spatial resolution.

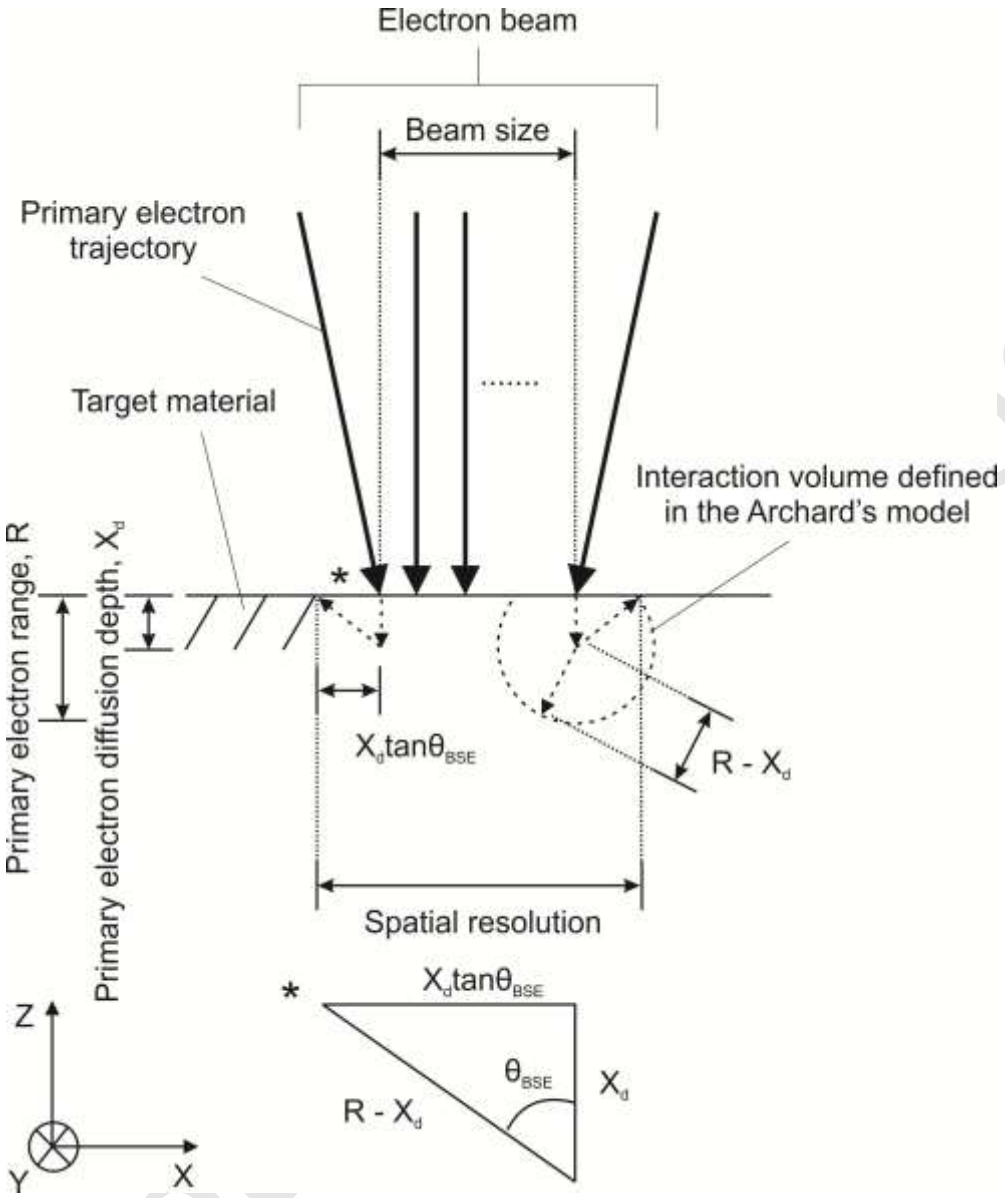

Fig. 3 Beam size and spatial resolution (without gas)

The definition of spatial resolution depicted in Fig. 3 makes use of the concept of BSE generation from Archard's model [22]. This model estimates that, the widest possible angle between the trajectory of a returning BSE and the normal of the target material's surface, is limited by the returning path length, $R - X_d$. This is the longest possible path taken by any BSE if it is to have sufficient energy to re-emerge from the target material (BSE energy is

consumed by inelastic collisions within the material). Table 1 summarises the estimation on the electron range using Eq. 1 [23], whilst Table 2 summarises the estimation on spatial resolution using Eq. 2 [22] with iron and aluminium being the imaging target materials. These were the two elements involved in this study.

$$R = \frac{(0.0276AE^{1.67})}{\rho Z_{target}^{0.89}} \quad (1)$$

Where

R (μm) is the electron penetration range into the imaging target material, A (amu) is the atomic mass of the material, ρ (gcm^{-3}) is the material density, Z_{target} is the atomic number of the material, and E (keV) is the primary electron energy.

Table 1 Electron range estimation. Data rounded to 3 significant figures (s.f.).

Parameter	Value for Iron Target	Value for Aluminium Target
E (keV)	60.0	
Z_{target}	26.0	13.0
A (amu)	56.0	27.0
ρ (gcm^{-3})	7.87	2.70
R (μm)	10.1	26.2

$$\frac{X_d}{R} = \frac{40}{7Z_{target}} \quad (2)$$

Where

X_d (μm) is the electron diffusion depth (complete electron diffusion occurs beyond this point)

Table 2 Spatial resolution estimation (without gas). Data rouned to 3 s.f.

Parameter	Value for Iron Target	Value for Aluminium Target
X_d (μm)	2.22	11.5
Half of the total width of BSE region affecting resolution, $X_d \tan\theta_{BSE}$ (μm)	7.56	9.16
Minimum electron beam size (mm)	0.200 [24]	
Spatial resolution without gas, $R_{sp\ (no\ gas)}$ (mm)	0.215	0.218

The spatial resolution analysis described above was estimated for situations with the absence of gas. However, the Arcam A1 EBM machine commonly operates under helium pressure at 2 x 10^{-3} mbar [25]. The influence of gas on spatial resolution is thought to be the broadening of the primary machine electron beam. This phenomenon is also known as "beam skirting" [26]. It is due to scattering of the electron beam by the gas molecules. The extent of skirting depends on parameters including, primary electron energy, type of gas, gas pressure, beam working distance, and gas temperature. Fig. 4 gives the definition of beam skirt radius [27] whilst Eq. 3 predicts its values [26]. Table 3 summarises the estimation on skirt radius when electronic imaging is conducted inside the A1 EBM machine at room temperature.

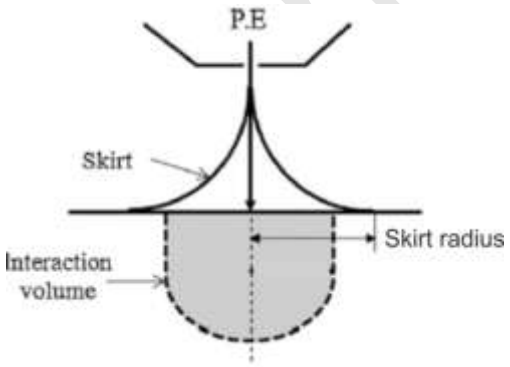

Fig. 4 Definition of electron beam skirt radius, adapted from [27]

$$r_{skirt} = \frac{364.19 Z_{gas}}{E}\left(\frac{P}{T}\right)^{\frac{1}{2}} {L_{W.D}}^{\frac{3}{2}} \quad (3)$$

Where

r_{skirt} (m) is the beam skirt radius, E (eV) is the primary electron beam energy, Z_{gas} is the atomic number of the gas present, P (Pa) is the pressure of the gas, T (K) is the gas temperature, and $L_{W.D}$ (m) is the working distance

Table 3 A1 EBM machine electron beam skirt radius estimation. Data rounded to 3 s.f

Parameter	Value
Z_{gas}	2.00
E (keV)	60.0
P (mbar)	2.00×10^{-3}
T (°C)	30.0
$L_{W.D}$ (mm)	400
r_{skirt} (mm)	0.0789

Table 2 gives an estimated spatial resolution of 0.215 to 0.218 mm, when electronic imaging is conducted on a titanium target with the absence of gas. The final spatial resolution with the influence of gas taken into account is calculated by Eq. 4. Table 4 summarises the estimation of the achievable spatial resolution of electronic imaging when conducted inside the A1 EBM machine at room temperature.

$$R_{sp} = R_{sp(no\ gas)} + 2r_{skirt} \quad (4)$$

Where

R_{sp} (mm) is the final spatial resolution, $R_{sp\ (no\ gas)}$ (mm) is the spatial resolution without gas, and r_{skirt} (mm) is the skirt radius due to the presence of helium gas at 2×10^{-3} mbar.

Table 4 Electron beam spatial resolution estimation (with gas). Data rounded to 3 s.f.

Parameter	Value for Iron Target	Value for Aluminium Target
$R_{sp(no\ gas)}$ (mm)	0.215	0.218
r_{skirt} (mm)	0.0789	
R_{sp} (mm)	0.373	0.376

2.2 Spatial Resolution Experimental Setup

Spatial resolution was investigated by conducting a knife edge test [15] with the use of electronic images generated by a custom digital electronic imaging system prototype developed for an Arcam A1 EBM machine [11]. Fig. 5 is the schematic of the prototype. The prototype consisted of a feedback electron sensor (modified Arcam heat-shield frame and plates), a data logger (Arduino DUE microcontroller break-out board), a signal amplifier and electronic image generation software.

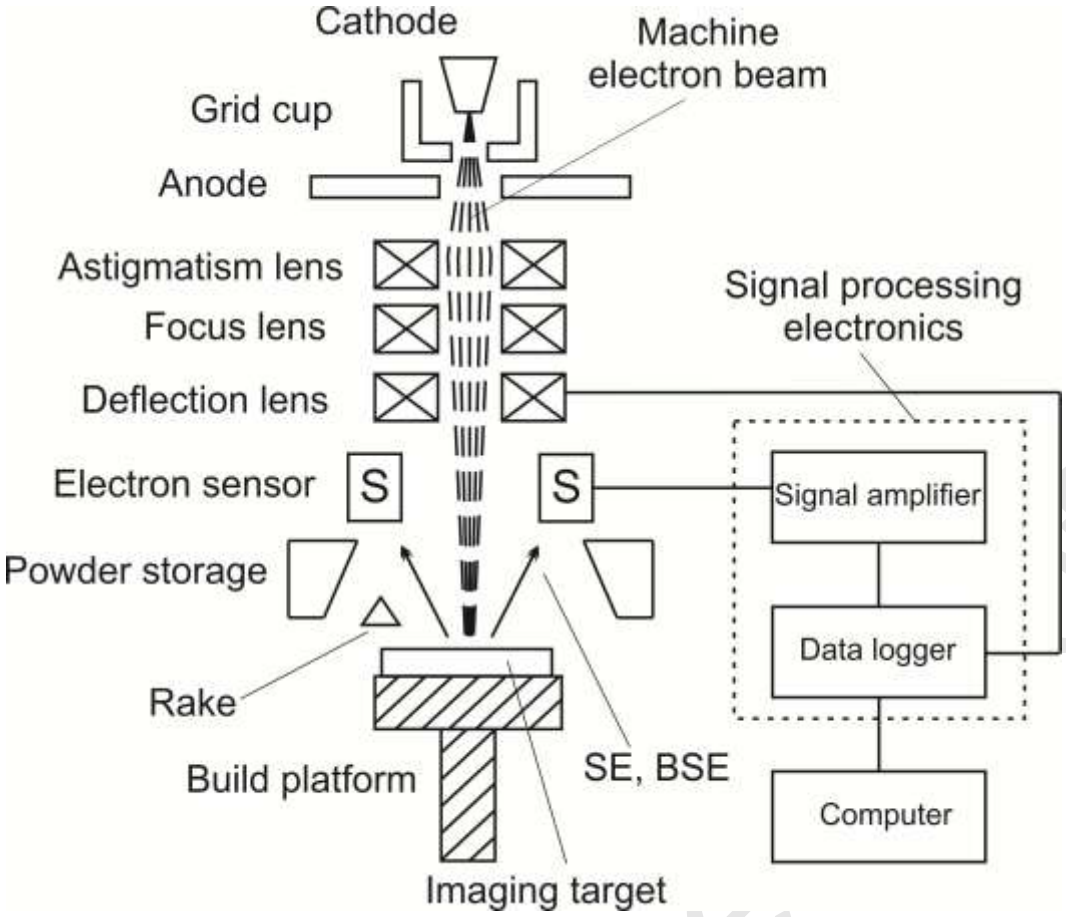

Fig. 5 Electronic imaging system prototype schematic [11]

In the experiments, the electron beam size was evaluated and used as an indicator for spatial resolution. A Grade 316 stainless steel plate (Merseyside Metal, UK) with 3M 1436 aluminium foil tape (3M, USA) applied, as shown in Fig. 6, was used as an imaging target in the experiment. The aluminium tape was used firstly, to create material contrast from the stainless steel plate, due to the sensitivity of feedback BSE signal yield on the atomic number of materials [28], and secondly, the edge of the tape was used to evaluate the electron beam size when the beam scans in a direction perpendicular to the tape edge. The custom electronic imaging system prototype was interfaced with the Arcam A1 EBM machine. Tables 5 and 6 summarise the electronic image settings and the configurations of both the EBM machine and the prototype.

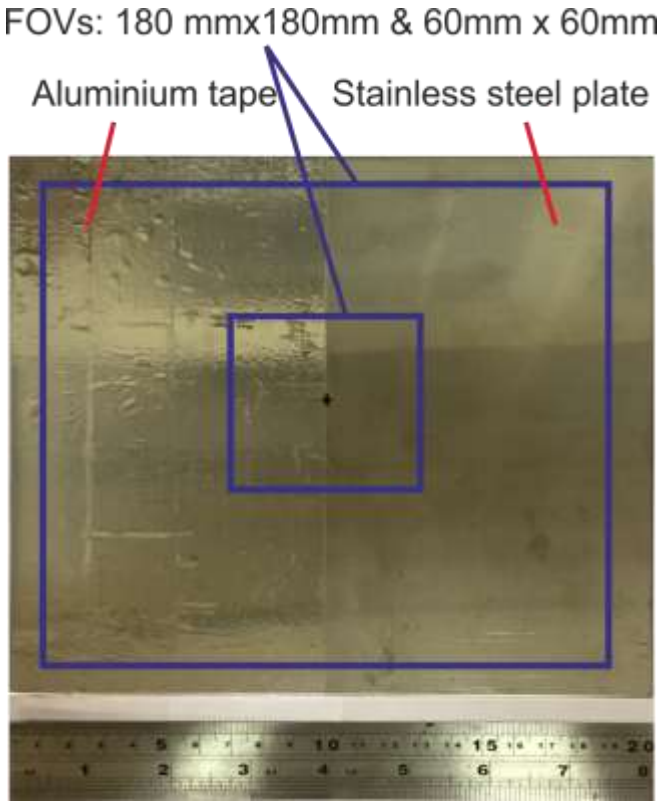

Fig. 6 Imaging target of the spatial resolution experiment

Table 5 Experiment image settings

Image Size (pixel)	Number of Images to Generate in Experiment	FOV (mm^2)	Pixel Resolution - ratio of FOV to image size (mm/pixel)
1800 x 1800	5	180 x 180	0.1
1800 x 1800	5	60 x 60	0.033

Table 6 Arcam A1 EBM machine and imaging prototype configurations

Parameter	Value
Beam current (mA)	1 (FOV: 180 x 180) 0.5 (FOV: 60 x 60)
Beam scan speed (mms^{-1})	11880
Chamber pressure (mbar)	2×10^{-3}
Signal amplifier gain	10
Data logger input / output range (V)	0 to +3.3
Data logger sampling frequency (Hz)	118.8k
Data logger sampling bit rate (bps)	950.4k
Imaging area (mm^2)	180 x 180 / 60 x 60
Raster-scan spacing (mm)	0.1 (FOV: 180 x 180) 0.033 (FOV: 60 x 60)
Image grayscale bit depth	2^8 (256)
Image frame time (s)	27.3

Once the raw electronic images were generated, pixel value profiles of four scan lines (pixel row index: 300, 600, 1200, and 1500) were extracted from each image for spatial resolution analysis. The central row (pixel row index: 900) of each image was deliberately avoided due to the damage on the aluminium tape incurred during one of the EBM machine setup procedures, i.e. beam centring. The spatial resolution of the electronic imaging system prototype was determined from the pixel value profile, based on the definition given in Fig. 1(b).

3. Results

Five raw electronic images were generated per FOV setting (180mm x 180mm and 60mm x 60mm). Fig. 7(a) shows the typical raw image with the four scan lines to be extracted for edge resolution analysis. Fig. 7(b) shows the typical pixel value ESF of an extracted scan line from the raw image, and the definition of spatial resolution, based on the definition given in Fig. 1(b). The pixel value data from the raw electronic images was best-fitted from linear regression [29] and the use of a modified standard hyperbolic tangent function, i.e. tanh(x), as detailed in Eq. 5. Image spatial resolution was then calculated based on Eq.6.

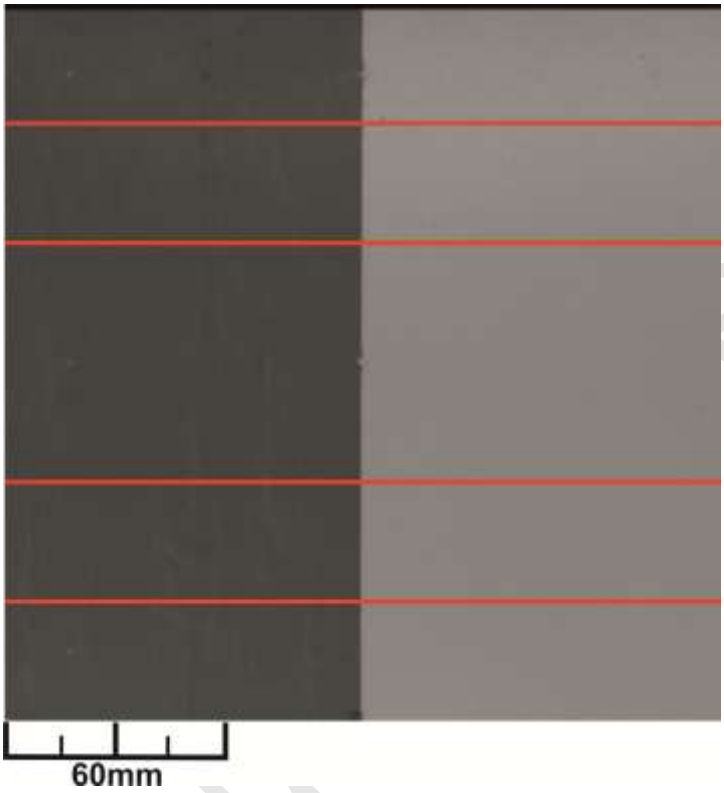

(a) Five scan lines for spatial resolution analysis

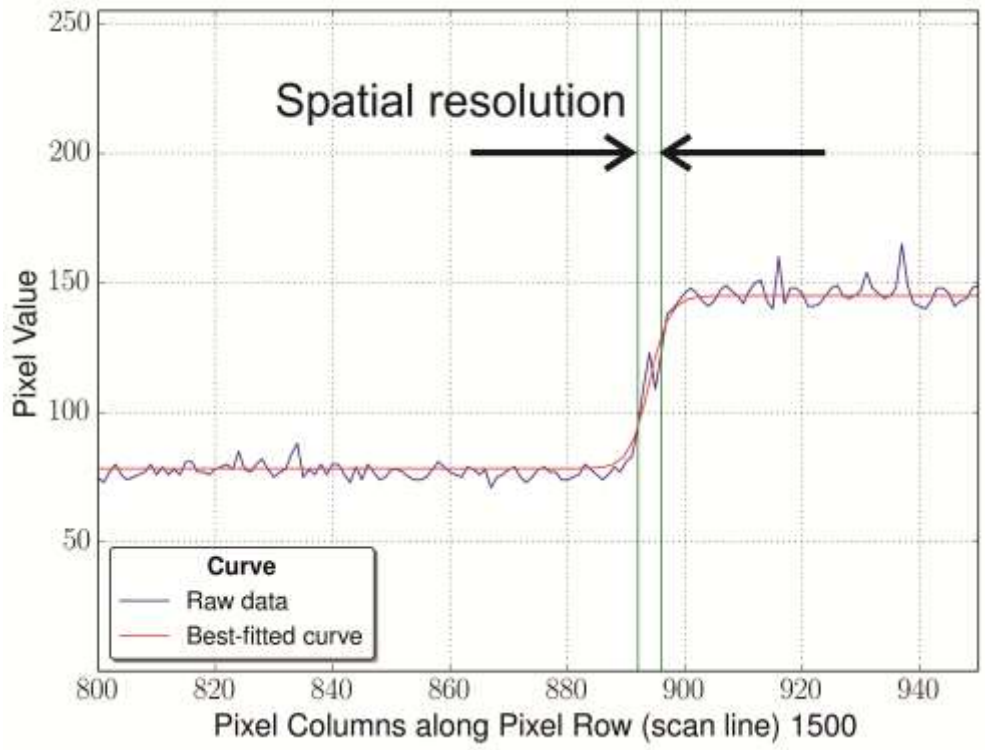

(b) Scan line pixel value ESF and the spatial resolution width

Fig. 7 Experimental result analysis

$$I(x) = A + B\tanh\left(\frac{x - C}{D}\right) \tag{5}$$

Where

I(x) is the pixel value of the selected scan line (pixel row), x is the pixel column index of the selected scan line. "A" to "D" are parameters used to modify the standard tanh(x) function: "A" controls the offset in pixel value, "B" controls the amplification in magnitude, "C" controls the offset in pixel column index, and "D" controls the spread of the function.

$$R_{sp} = \Delta Img_{Col} \times \frac{Img_{width,mm}}{Img_{width,pixel}} \tag{6}$$

Where

R_{sp} (mm) is the pixel value, ΔImg_{Col} (pixel) is the number of pixels between two pixel columns with 25% and 75% of the maximum pixel values, $Img_{width,mm}$ (mm) and $Img_{width,pixel}$ are the electronic image 1D size (i.e. 60 mm, 180 mm and 1800 pixels).

Fig. 8 and Table 7 give the experimental and spatial resolution analysis results for electronic images with FOV of 180 mm x 180 mm, whilst Fig. 9 and Table 8 give results for images with FOV of 60 mm x 60 mm. Figs. 8 and 9 indicate that the pixel value profiles from images with a FOV of 180 mm x 180 mm have greater Signal-Noise-Ratio (SNR). Fig. 10 visually presents the results summarised in Table 7 and 8. No observable trend can be drawn from Fig. 10, between data from the two different FOVs.

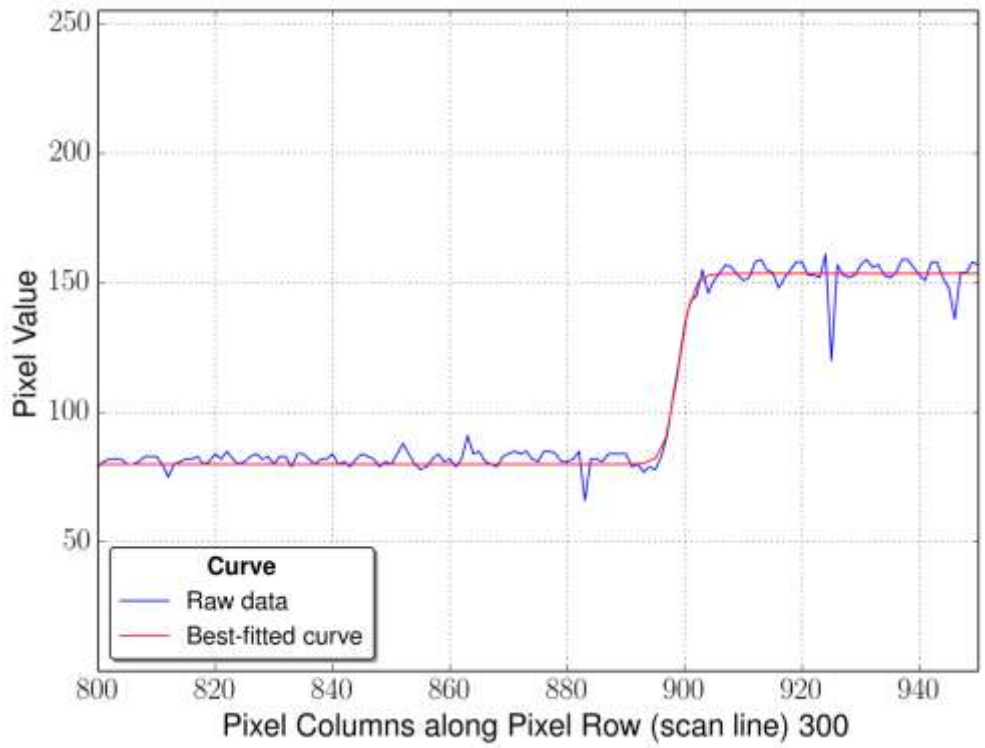

Fig. 8 Typical result of images with FOV of 180 mm x 180 mm, scan line pixel value ESF

Table 7 Spatial resolution result (FOV: 180 mm x 180 mm). Data rounded to 3.s.f.

Electronic Image Sample Number	R_{sp} /mm	Standard Error
1	0.350	0.0224
2	0.275	0.0194
3	0.300	0.0316
4	0.325	0.0194
5	0.350	0.0500

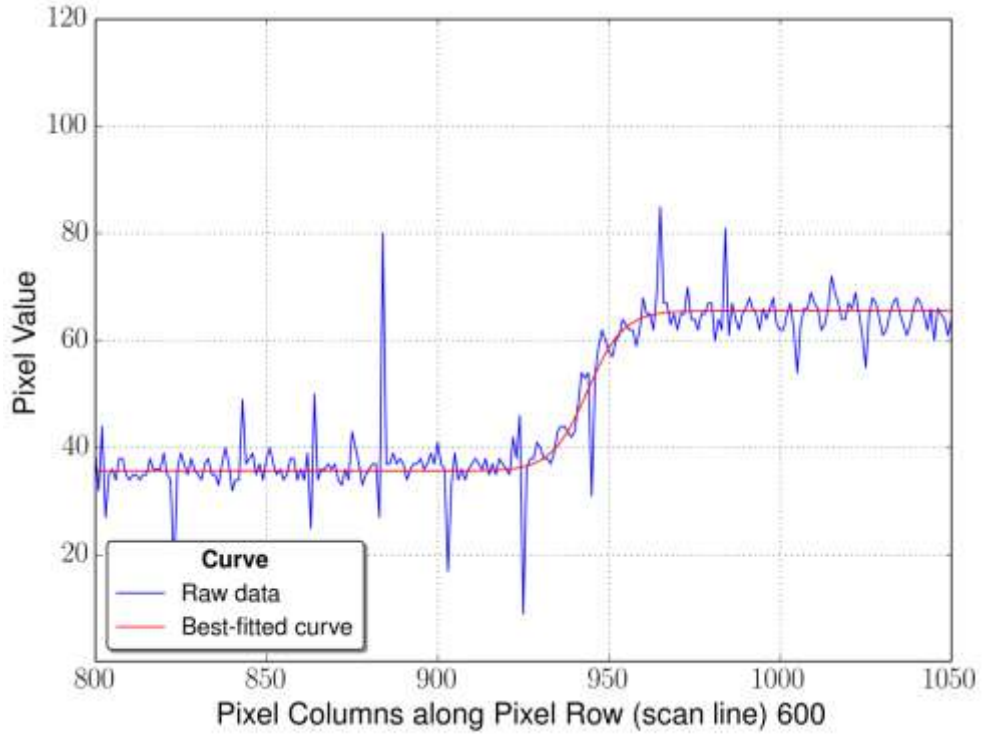

Fig. 9 Typical result of images with FOV of 60 mm x 60 mm, scan line pixel value ESF

Table 8 Spatial resolution result (FOV: 60 mm x 60 mm). Data rounded to 3.s.f.

Electronic Image Sample	R_{sp} /mm	Standard Error
1	0.275	0.0286
2	0.383	0.0373
3	0.350	0.0373
4	0.408	0.0194
5	0.375	0.0286

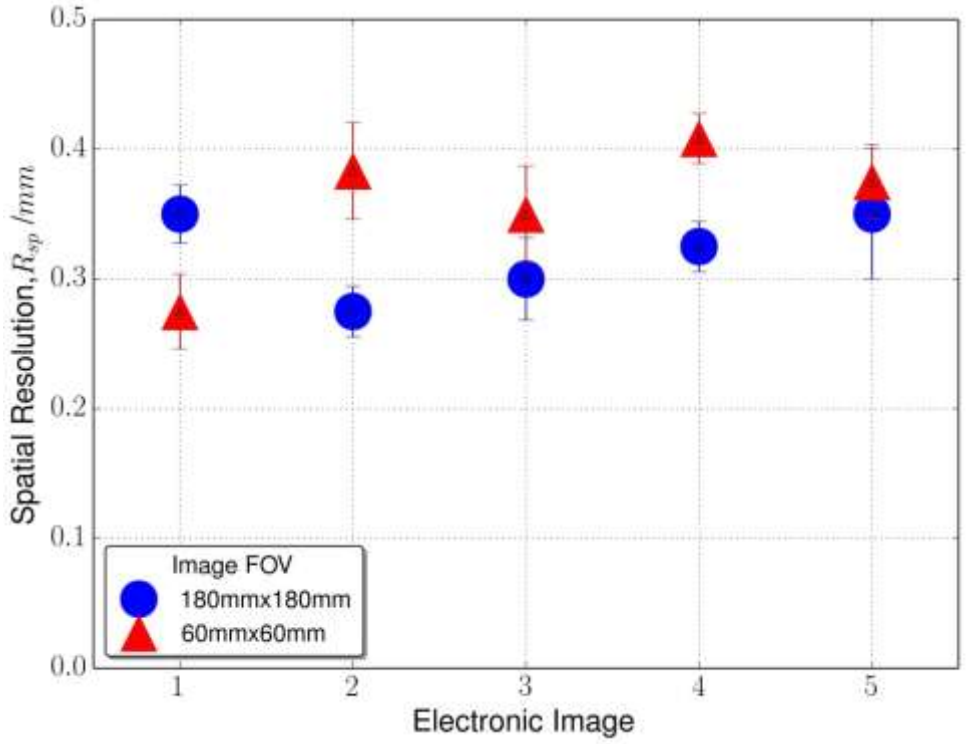

Fig. 10 Edge spatial resolution analysis result

4. Discussion

4.1 Differences in Electronic Image Quality with Different Image FOVs

Variations in SNR are seen from Figs. 8 and 9. It is postulated that the differences in image contrast and SNR both stem from the electron beam current settings when electronic imaging was carried out during the experiment. Table 6 shows that a beam current of 1 mA was used for images with FOV of 180 mm x 180 mm , whilst 0.5 mA was used for images with FOV of 60 mm x 60 mm. Table 6 also indicates that the image frame time was 27.3 s for all images regardless of their FOVs. The fixed image frame time led to more severe electron beam heating of the imaging target during the imaging of a smaller area. Heating of the target might lead to damage of the aluminium tape, and thus the beam current was set to 0.5 mA for the 60 mm x 60 mm imaging area. The first drawback of this approach is that, the reduced electron beam current led to a reduction in feedback electron signal strength, leading to less signal contrast for the electronic images with a FOV of 60 mm x 60 mm when compared to the result with a FOV of 180 mm x 180 mm. In addition, the second drawback is the

deterioration in the image signal SNR. Shot noise is a common type of noise in electronic imaging. Reimer [30] reported that the primary electron beam has a statistical distribution when hitting the specimen during a given image pixel time. As SE and BSE are generated from the interaction between the primary electrons and the specimen, they too exhibit similar distribution, which manifests itself as shot noise in the feedback electron signal. Ul-Hamid gave the SNR expression, as shown in Eq. 7 [31], which indicates that the SNR increases with the average signal level. When comparing with the setting for FOV of 180 mm x 180mm, the reduction in beam current for FOV of 60 mm x 60 mm led to a decrease in feedback electron signal strength. As a result, the SNR reduced, as observed when comparing Fig. 9 with Fig. 8 (pixel value is proportional to signal strength).

$$SNR = \frac{Signal}{Noise} = \frac{n}{\sqrt{n}} = \sqrt{n} \tag{7}$$

Where

n (mA) is the average strength of the signal

4.2 Spatial Resolution – Estimation and Experimental Results

Referring to Tables 7 and 8, the average spatial resolution estimated for images with an FOV of 180 mm x 180 mm and 60 mm x 60 mm are 0.320 mm and 0.358 mm. Firstly, these values are of the same order of magnitude when compared with the minimum achievable beam size of 0.2 mm claimed by Arcam AB [24] and the spatial resolution of 0.373 to 0.376 mm estimated in Table 4. This verifies the validity of the experimental setup and data analysis method.

Secondly, it is thought that results imply that the impasse of the spatial resolving power in this study lies with the machine electron beam size. Table 5 shows that for images with FOV of 60 mm x 60 mm, the pixel resolution is 0.033 mm. This indicates that if an infinitely small machine electron beam were available, the measured spatial resolution should be expected to be of the order of 0.033 mm, rather than the observed 0.358 mm.

5. Conclusions

This article has proposed a new indicator for spatial resolution by taking into account the effect of BSE information depth on top of the size of an electron beam, for electronic imaging

conducted inside an Arcam A1 EBM machine. Theoretical analysis of the achievable spatial resolution was carried out and 0.373 to 0.376 mm was estimated to be the resolution when considering the influence of the presence of helium gas at 2 x 10^{-3} mbar inside the EBM machine chamber. In addition, this study suggests a method to carry out a knife edge test with the use of a custom electronic imaging system prototype, operating at room temperature, inside an EBM machine. Spatial resolution was evaluated at two image FOV settings, i.e. 180 mm x 180 mm and 60 mm x 60 mm, and the observed resolution are 0.320 mm and 0.358 mm respectively. However, in order to realise this in-process monitoring potential of electronic imaging, further spatial resolution studies need to be carried out at elevated, in-process EBM temperatures for various popular AM materials. It is believed that this study has contributed to the on-going development of an in-process EBM monitoring system, by providing a method to analyse and benchmark the achievable spatial resolution of an electronic imaging system, which operates inside an EBM machine at room temperature.

Conflict_of_interest

The Author(s) declare(s) that there is no conflict of interest. This research received no specific grant from any funding agency in the public, commercial, or not-for-profit sectors. The EBM machine was purchased, in part from a grant received for the EPSRC Centre for Innovative Manufacturing in Additive Manufacturing, EP/I033335/2.

Acknowledgements

The Author(s) declare(s) that there is no conflict of interest. This research received no specific grant from any funding agency in the public, commercial, or not-for-profit sectors. The EBM machine was purchased, in part from a grant received for the EPSRC Centre for Innovative Manufacturing in Additive Manufacturing, EP/I033335/2.

References

[1] I. Gibson, D.W. Rosen, B Stucker (2010) Additive Manufacturing Technologies. Springer, New York, pp. 126-128

[2] G. Baudana, S. Biamino, D. Ugues, M. Lombardi, P. Fino, M. Pavese, C. Badini, (2016) Titanium Aluminides for Aerospace and Automotive Applications Processed by Electron Beam Melting: Contribution of Politecnico di Torino, Metal Powder Report,

Volume 71, Issue 3, 2016, Pages 193-199, ISSN 0026-0657, http://dx.doi.org/10.1016/j.mprp.2016.02.058.

[3] O.L.A Harrysson, O. Cansizoglu, D.J. Marcellin-Little, D.R Cormier, H.A West (2008) Direct Metal Fabrication of Titanium Implants with Tailored Materials and Mechanical Properties using Electron Beam Melting Technology, Materials Science and Engineering: C, Volume 28, Issue 3, 2008, Pages 366-373, ISSN 0928-4931, http://dx.doi.org/10.1016/j.msec.2007.04.022.

[4] X Gong, T Anderson, K Chou (2014) Review on Powder-Based Electron Beam Additive Manufacturing Technology. Manufacturing Review 1 2. DOI: 10.1051/mfreview/2014001

[5] National Institutio of Standards and Technology, U.S. Department of Commerce (2013) Measurement Science Roadmap for Metal-Based Additive Manufacturing Workshop Summary Report, Pages 61-70, https://www.nist.gov/sites/default/files/documents/el/isd/NISTAdd_Mfg_Report_FINAL-2.pdf

[6] X. Tan, Y. Kok, S.B Tor, C.K Chua (2014) Application of Electron Beam Melting (EBM) in Additive Manufacturing of an Impeller, Proc. of the Intl. Conf. on Progress in Additive Manufacturing, doi:10.3850/978-981-09-0446-3 076

[7] S. Everton, M. Hirsch, P. Stravroulakis, R. Leach, A. Clare (2016) Review of In-Situ Process Monitoring and In-Situ Metrology for Metal Additive Manufacturing, Materials and Design 95 (2016) pp. 431–445, http://dx.doi.org/10.1016/j.matdes.2016.01.099

[8] W.J. Sames V (0215) Additive Manufacturing of Inconel 718 Using Electron Beam Melting: Processing, Post-Processingm and Mechanical Properties, PhD Thesis, Texas A&M University

[9] M. Mani, B. Lane, A. Donmez, S. Feng, S. Moylan, R. Fesperman (2015) NISTIR 8036. Measurement Science Needs for Real-time Control of Additive Manufacturing Powder Bed Fusion Processes. http://dx.doi.org/10.6028/NIST.IR.8036

[10] C. Arnold, C. Pobel, F. Osmanlic, C. Körner (2018) Layerwise monitoring of electron beam melting via backscatter electron detection. Rapid Prototyping Journal 24/8 (2018) 1401–1406. DOI 10.1108/RPJ-02-2018-0034

[11] H. Wong, D. Neary, S. Shahzad, E. Jones, P. Fox, C. Sutcliffe (2018) Pilot Investigation of Feedback Electronic Image Generation in Electron Beam Melting and its Potential for In-Process Monitoring, Elsevier Journal of Materials Processing Technology, DOI: 10.1016/j.jmatprotec.2018.10.016

[12] H. Wong, D. Neary, E. Jones, P. Fox, C. Sutcliffe (2018) Pilot capability evaluation of a feedback electronic imaging system prototype for in-process monitoring in electron beam additive manufacturing, Springer International Journal of Advanced Manufacturing Technology, DOI: 10.1007/s00170-018-2702-6

[13] H. Wong, D. Neary, S. Shahzad, E. Jones, P. Fox, C. Sutcliffe (2018) Pilot Feedback Electronic Imaging at Elevated Temperatures and its Potential for In-Process Electron Beam Melting Monitoring, Elsevier Additive Manufacturing (in-press)

[14] G.F. Lorusso, D.C Joy (2003) Experimental Resolution Measurement in Critical Dimension Scanning Electron Microscope Metrology, SCANNING VOL. 25, pp. 175–180 (2003)

[15] L. Reimer (1998) Scanning Electron Microscopy: Physics of Image Formation and Microanalysis, Springer, pp. 4 – 5

[16] A. Kaur, C. Ribton, W. Balachandaran (2015) Electron Beam Characterisation Methods and Devices for Welding Equipment, Elsevier Journal of Materials Processing Technology, http://dx.doi.org/10.1016/j.jmatprotec.2015.02.024

[17] J.W. Elmer (2009) Characterization of Defocused Electron Beams and Welds in Stainless Steel and Refractory Metals using the Enhanced Modified Faraday Cup Diagnostic, LLNL-TR-410110, DOI: 10.2172/947235

[18] A. Stratan, A. Zorila, L. Rusen,G. Nemes (2014) Measuring Effective Area of Spots From Pulsed Laser Beams, Optical Engineering 53(12), 122513, DOI: 10.1117/1.OE.53.12.122513

[19] M.A. C. de Araújo, R. Silva, E. de Lima, D.P. Pereira, P.C. de Oliveira1 (2009) Measurement of Gaussian Laser Beam Radius using the Knife-Edge Technique: Improvement on Data Analysis, APPLIED OPTICS Vol. 48, No. 2

[20] Course PH5060, Teaching Materials, Department of Physics, Indian Institute Of Technology Madras , Chennai, http://www.physics.iitm.ac.in/~ph5060/manuals/Gaussianlaserbeam.pdf

[21] J. Tragardh, K. Macrae, C. Travis, R. Amor, G. Norris, S.H. Wilson, G.L. Oppo, G. Mcconnell (2015) A Simple but Precise Method for Quantitative Measurement of the Quality of the Laser Focus in a Scanning Optical Microscope, Journal ofMicroscopy, Vol. 259, Issue 1 2015, pp. 66–73, doi: 10.1111/jmi.12249

[22] G.D Archard (1961) Back Scattering of Electrons, Journal of Applied Physics 32, 1505 (1961); doi: 10.1063/1.1728385

[23] S. Okayama, K. Kanaya (1972) Penetration and Energy-Loss Theory of Electrons in Solid Targets. Journal of Physics D: Applied Physics, Vol. 5, Issue 1, pp. 43-58, doi: 10.1088/0022-3727/5/1/308

[24] Arcam A1 EBM Machine Specification, http://www.arcam.com/wp-content/uploads/Arcam-A1.pdf

[25] P. Wang, W. Sin, M.L. Nai, J. Wei (2017) Effects of Processing Parameters on Surface Roughness of Additive Manufactured Ti-6Al-4V via Electron Beam Melting, Materials 2017, 10, 1121; doi:10.3390/ma10101121

[26] G.D. Danilatos (1988) Foundations of Environemtal Scanning Electron Microscopy, Advances in Electronics and Electron Physics ,Vol. 71, Academic Press, Inc. ISBN 0-12-014671-1, pp. 162

[27] A. Zoukel,L. Khouchaf, J.Di. Martino, D. Ruch (2012) Skirting effects in the variable pressure scanning electron microscope: Limitations and improvements, Micron 44 (2013) pp. 107–114, http://dx.doi.org/10.1016/j.micron.2012.05.004

[28] L. Reimer (1998) Scanning Electron Microscopy: Physics of Image Formation and Microanalysis, Springer, pp. 135-148

[29] D. Auroux (2010) 18.02SC Multivariable Calculus. Massachusetts Institute of Technology: MIT OpenCourseWare, https://ocw.mit.edu. License: Creative Commons BY-NC-SA. Course notes on " Least Square Interpolation"

[30] L. Reimer (1998) Scanning Electron Microscopy: Physics of Image Formation and Microanalysis, Springer, pp. 165 – 166

[31] A. Ul- Hamid (2018) A Beginners' Guide to Scanning Electron Microscopy, Springer, pp. 82